Development of Fractal 5G MIMO Antenna for Sub 6 GHz Wireless Automotive Applications

Ashish Kumar[1], Gurmeet Singh[2], Muhannad K. Abdulhameed[3, 4],
Sarah R. Hashim[5], and Ahmed J. A. Al-Gburi[6, *]

[1]*Chitkara University Institute of Engineering and Technology, Chitkara University, Punjab, India*
[2]*School of Computer Science and Engineering, Galgotias University, Uttar Pradesh, India*
[3]*Computer Scince Department, University of Kerbala, Karbala, Iraq*
[4]*Air Conditioning Engineering Department, Faculty of Engineering, Warith Al-Anbiyaa University, Iraq*
[5]*Department of Cyber Security, Al-Zahraa University for Women, Karbala, Iraq*
[6]*Center for Telecommunication Research & Innovation (CeTRI)*
Fakulti Teknologi dan Kejuruteraan Elektronik dan Komputer (FTKEK)
Universiti Teknikal Malaysia Melaka (UTeM), Jalan Hang Tuah Jaya, Durian Tunggal, Melaka 76100, Malaysia

ABSTRACT: Multi-input multi-output (MIMO) antennas have garnered significant attention for addressing the demands of high channel capacity, reliable and uninterrupted signal transmission, and high data rates, especially with recent advancements in 5G low Earth orbit (LEO) satellite communications. In addition to these features, automotive applications require antennas with minimal mutual coupling, high gain, multiple resonant frequencies, and compact size for user equipment. To meet these requirements, a 1×2 defected ground structure (DGS)-based fractal MIMO antenna array is proposed, covering various frequencies in the sub-6 GHz bands, including 0.7 GHz, 2.6 GHz, 3.1 GHz, and 3.5 GHz. The proposed antenna provides sufficient channel bandwidths and achieves a gain of 12.9 dBi in the n78 frequency band. The design has been fabricated, and the measured results show good agreement with the simulated ones. Moreover, the proposed antenna design can be integrated into the plastic parts of a car body, offering various automotive applications. It achieves a realistic data rate of approximately 10–12 Mbit/s, as verified through link budget calculations that consider the key parameters of LEO satellite systems.

1. INTRODUCTION

The recent advancements in wireless communication indicate the need for higher channel capacity, reliable and uninterrupted connections for extended durations, system stability, and higher data rates [1]. All these features have been explored in introducing the 5th generation (5G) new radio (NR) releases by 3rd generation partnership project (3GPP) [2]. Among the above-mentioned features, high data rate and free space path loss play a significant role in efficient and uninterrupted wireless communication in rural areas while travelling in the automobiles. Moreover, due to recent developments in the newly launched LEO satellite ventures like star link, one web, and amazon, the free space path loss decreases significantly as the orbital height of these satellites is in the range of 250–500 km [3]. This will provide the advantage to design compact and medium gain user equipment antennas which can be easily integrated with mobile phones or plastic parts of the modern passenger car. Further, high data rate will depend upon the choice of frequencies for efficient 5G communication. According to 3GPP new releases, sub-6 GHz and mm-wave frequency bands have been selected for the 5G communication [4, 5].

Further, these bands include n77/78/70 band (3.3 to 5 GHz) and n257 band (26.5 to 29.5 GHz) [6]. These bands have

been selected on the basis of various key performance indicators like uplink and downlink data rate, antenna size, transmitter/receiver cost, corresponding chipset availability and electromagnetic compatibility [7]. It is required to introduce geometrical perturbations in the patch antenna to cover multiple frequencies in these bands and other 5G frequency bands, which can cause further current distribution variation on the radiating patch. In view of this, fractal structure is one of the prominent solutions to address the issues of multiple frequencies [8–11]. In this direction, various researchers have put their efforts like in [12], and a spiral-shaped MIMO antenna is proposed for various low frequency bands like Wi-Fi, Wi-Max, etc. The performance has been improved by utilizing DGS. Similarly, a four-port MIMO structure is designed to operate at mm-wave frequency bands. In this structure, DGS has been implemented to achieve the gain of the antenna up to 8.3 dBi [13]. A wideband four element MIMO antenna on a flexible transparent substrate has been discussed in [14]. The proposed design covers a wide bandwidth of 92.32% with a low gain of only 0.53 dB. In a similar research, an 8-port MIMO antenna has been proposed for ultra-wideband (UWB) coverage of the frequency bands. Again, a modification is proposed in the ground layer to recover the mutual coupling among the patch elements [15]. In another research article, a series of slots have been etched into the ground plane to recover the coupling among the four radi-

* Corresponding author: Ahmed Jamal Abdullah Al-Gburi (ahmedjamal@ieee.org, engahmed_jamall@yahoo.com).
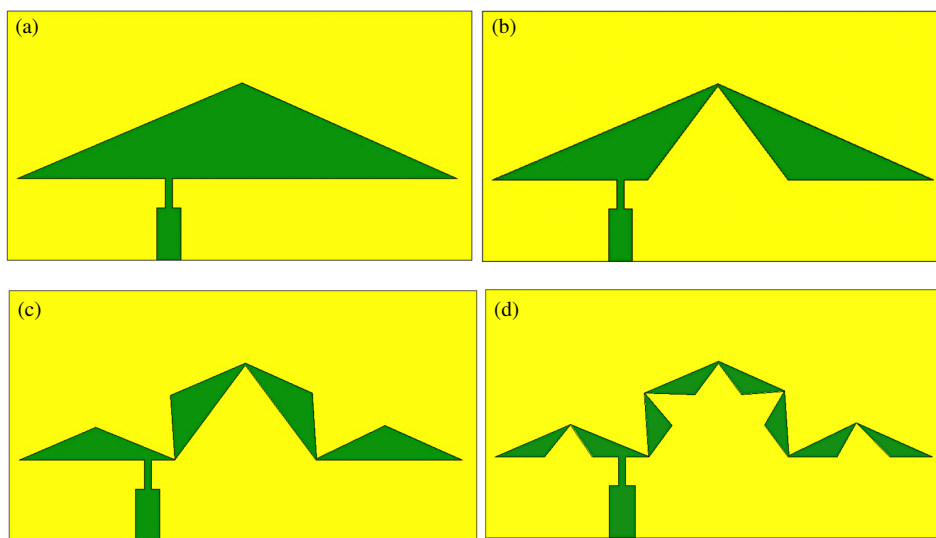
FIGURE 1. Proposed fractal antenna (FFA) iterations, (a) 0th, (b) 1st, (c) 2nd, (d) 3rd (Metal: Green color, Substrate: Yellow color).

ating antennas designed on the top of the substrate. The design covers the narrow bandwidth and resonates for the entire 2.4 GHz frequency band [16].

From the above discussion, it can be inferred that numerous authors have experimentally demonstrated MIMO antennas incorporating DGSs on the bottom plane to reduce mutual coupling and enhance performance parameters. However, most existing designs primarily cover frequency ranges starting from WLAN applications and extending to the UWB spectrum. In contrast, this article proposes a fractal antenna structure in a 2-element MIMO configuration, which not only covers sub-6 GHz frequency bands but also includes a resonating frequency at 700 MHz. The structure of the paper is as follows. Section 2 discusses the proposed design considerations. Section 3 presents the results and analysis, and Sections 4 and 5 provide the measured results and conclusions, respectively.

2. PROPOSED ANTENNA DESIGN

The proposed MIMO antenna design begins with a unit fractal element. The initial (0th) iteration starts with a triangular patch antenna, which is designed using Equation (1). Subsequent iterations ensure that the final design covers all the frequencies of interest, as outlined in [17]. The final iteration of the fractal antenna is developed on an FR4 substrate with a dielectric constant of $\varepsilon_r = 4.4$, a thickness of 1.6 mm, and a loss tangent ($\tan \delta$) of 0.02. All iterations of the proposed single-element fractal antenna are illustrated in Figure 1. In the literature, this design is referred to as a fractal antenna, constructed using the Iterated Function System (IFS) method. Figure 1(a) represents the initial stage of the design, while the final iteration is achieved by combining two scaled-down versions of the preceding shape. The attractor, denoted as D, represents the set where all subsets D_0 intersect, forming the fractal pattern. This process is mathematically described by Equations (2) to (4), as referenced in [17]. This iterative approach ensures a compact

and efficient design capable of covering the targeted frequency bands. Here the counteractivities of two identical duplicates $= \sqrt{5/4}$

$$s = \frac{2c}{3f_r\sqrt{\varepsilon_r}} \tag{1}$$

$$D = \bigcap_{i=1}^{\infty} D_i \tag{2}$$

$$D_n = f_1(D_{n-1}) \cup f_2(D_{n-1}) \tag{3}$$

$$D_0 \supset D_1 \supset D_2 \supset ... \supset D_{n-1} \supset D_n \tag{4}$$

The proposed antenna design is excited by microstrip line feeding matching the 50 Ω port impedance and edge of the radiating element. Moreover, the feed line has been shifted from the center position to the negative Y direction due to design requirements as the 1st iteration demands a cut at central part of the triangle. The dimensional pictorial view of the proposed design can be seen in Figure 2(a), and the side view of the proposed design can be visualized in Figure 2(b). All the dimen-

TABLE 1. Design specifications of fractal antenna.

Specifications	Value in mm
Length of the substrate (L_{sub})	52
Width of the substrate (W_{sub})	97
Side length of triangle (a)	17.2
Side length of triangle (b)	10.5
Side length of the triangle cut (c)	8.11
Vertical length of the triangle (d)	13.3
Quarter wave transformer feed length (F_{ql})	6
Quarter wave transformer feed width (F_{qw})	1.5
Feed width (F_W)	5.5
Feed length (F_L)	11

TABLE 2. Various output characteristics of the proposed FFA.

Iterations	Frequency (GHz)	Bandwidth (MHz)	Fractional bandwidth (%)	S_{11} (dB)
0th Iteration	1.17	82	7	-13 dB
	5.2	155	2.98	-12
1st Iteration	0.69	105	15.21	-16.4
	2.22	20	1.2	-10.7
	3.18	52	1.7	-12.3
2nd Iteration	0.69	—	—	-8
	1.9	—	—	-4
	3.5	103	2.9	-15.2
3rd Iteration	0.59	57	9.66	-11
	1.9	97	5.1	16
	2.6	70	2.69	-12
	3.1	71	2.29	-13
	3.57	117	3.27	-20
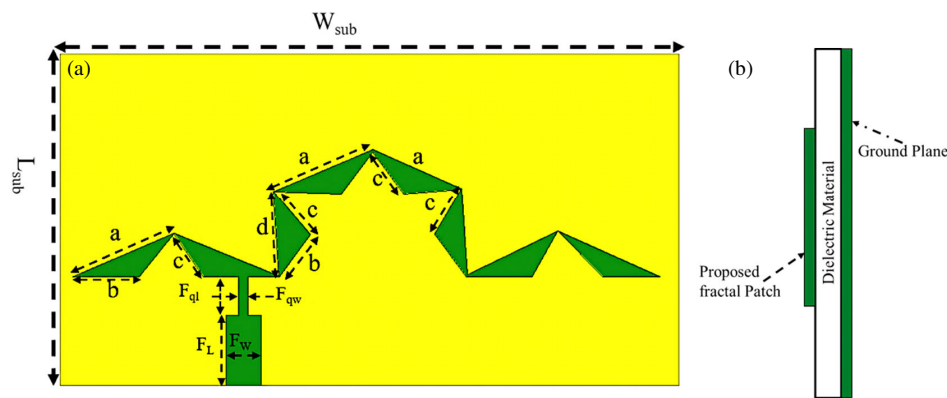
FIGURE 2. Dimensions of the proposed fractal antenna. (a) Top view with geometrical descriptions. (b) Side view.

sional specifications of the proposed FFA are illustrated in Table 1. The width of the substrate is slightly extended, because the lowest resonating frequency is very small. The resonance characteristics of the design are shown in Figure 3, which illustrates that 0th iteration does not provide any resonance in the sub-6 GHz frequency band. Then in the 1st iteration, resonance is achieved at 0.7 GHz but still not all the frequencies of interest. Similarly in the 2nd iteration, three resonating frequencies have been achieved, but with poor impedance matching. Therefore, in the final iteration, all the required multiple resonating frequencies with excellent impedance matching have been achieved. These frequencies include 0.69–0.74 GHz (n12), 1.9 GHz (n2), 2.6 GHz (n41), and 3.5 GHz (n78) [18]. Moreover, the 3.57 GHz resonating frequency covers the required channel bandwidth $B_{ch} = 100$ MHz. All the performance parameters of all the iterations are illustrated in Table 2.

The current distribution of the proposed design at different frequencies can be visualized in Figure 4 which shows that current is more dominated only on the left side of the design at the lowest frequency of operation, but as the frequency increases, the current distributes to the other portion of the design. At 1.9 G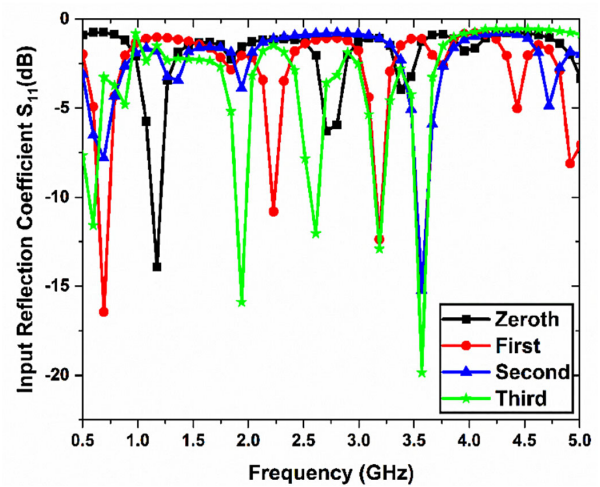Hz, the current at central and right parts of the design dominate as compared to the left part. Similarly at 3.5 GHz, the current distributes evenly on all the parts of the proposed design.

FIGURE 3. Simulated reflection coefficient variation with frequency of the proposed FFA.
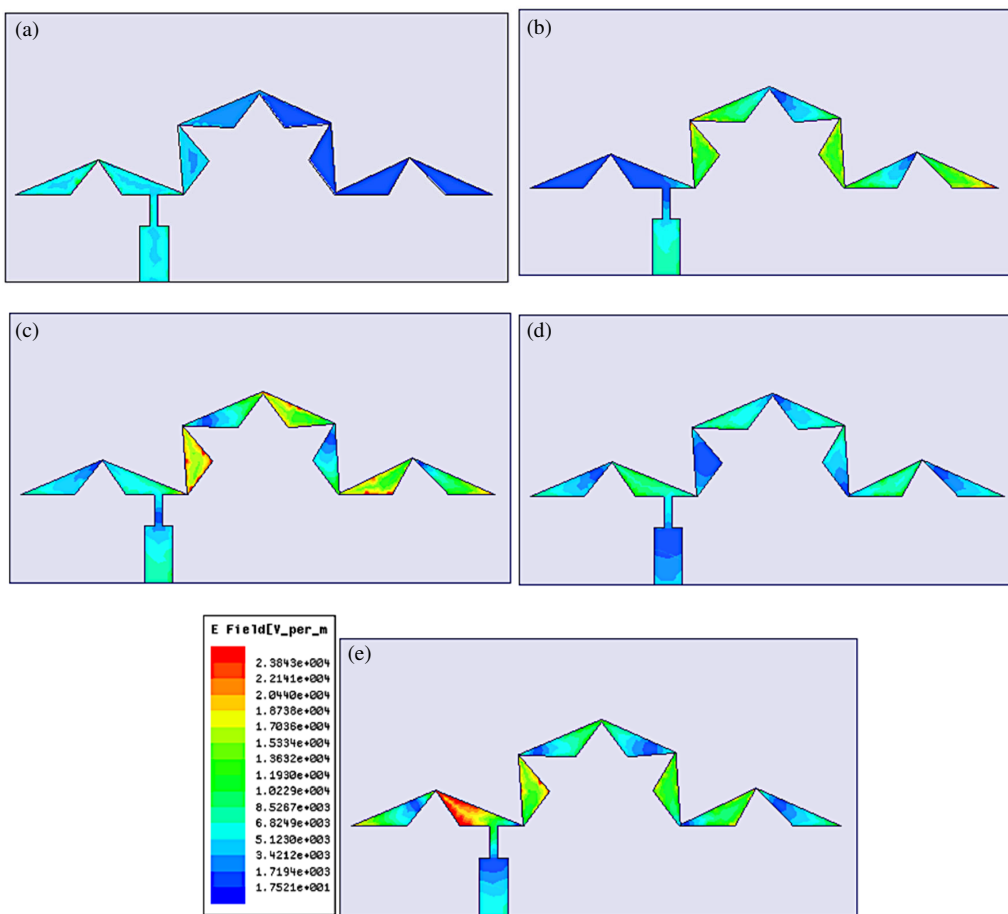
FIGURE 4. Current distribution of the proposed FFA at different frequencies in GHz, (a) 0.6 GHz, (b) 1.9 GHz, (c) 2.6 GHz, (d) 3.1 GHz, (e) 3.5 GHz.
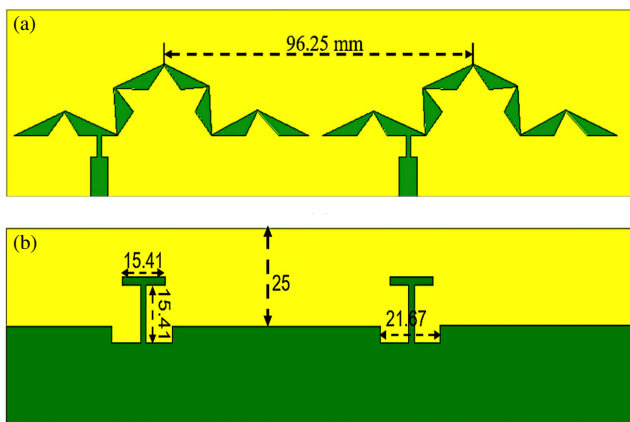

FIGURE 5. Proposed FFA MIMO configuration. (a) Top view. (b) Bottom view (All dimensions are in mm).

The finalized unit cell radiating element is transformed into 1×2 MIMO array structure as shown in Figure 5. The two elements are placed at $\lambda/2$ distance to avoid coupling among the elements. The overall size of the design would be $195\,\text{mm} \times 52\,\text{mm}$. Ground plane has been modified as shown in Figure 5(b) to improve the output parameters like impedance matching and gain.

3. RESULT AND ANALYSIS

Figure 6 illustrates the variation of the input reflection coefficient with respect to frequency and coupling, highlighting a significant improvement in the reflection coefficient upon the introduction of the defected ground structure (DGS). This enhancement also results in improved bandwidth, particularly at $0.6\,\text{GHz}$. Additionally, the mutual coupling (S_{12}) is observed to be less than $-20\,\text{dB}$ across the entire resonating frequency range, ensuring effective isolation between the MIMO antenna elements. Beyond these parameters, other critical metrics, such as envelope correlation coefficient (ECC), directive gain (DG), and channel capacity loss (CCL), must be evaluated to comprehensively assess the overall performance of the MIMO antenna configuration. These metrics are essential for determining the antenna's suitability for high-performance communication systems.

3.1. Envelope Correlation Coefficient (ECC)

The coupling can also be examined in terms of ECC which is represented by Equation (5) [12, 21, 22].

$$\rho_s = \frac{\left| S_{11}^* S_{12} + S_{21}^* S_{22} \right|^2}{\left(1 - |S_{11}|^2 - |S_{21}|^2 \right) \left(1 - |S_{22}|^2 - |S_{21}|^2 \right)} \quad (5)$$
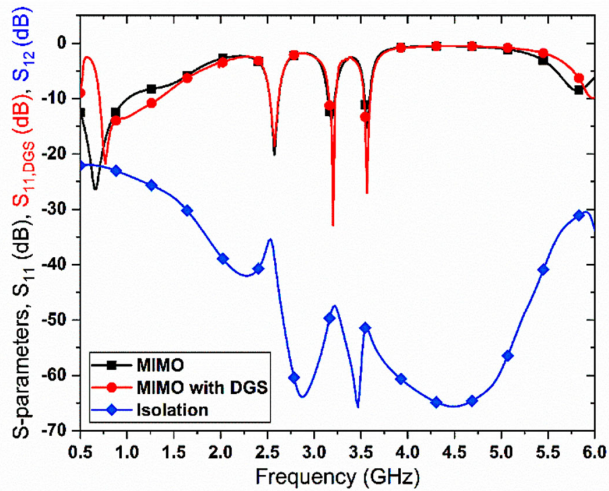
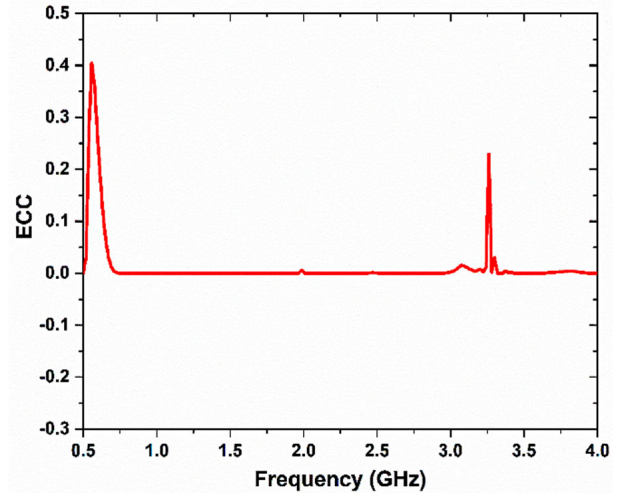FIGURE 6. S-parameters of the proposed FFA MIMO antenna.

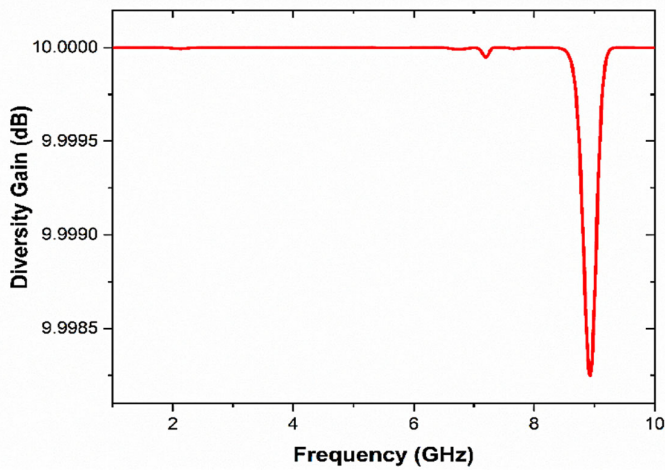FIGURE 7. Simulated ECC variations with frequency.
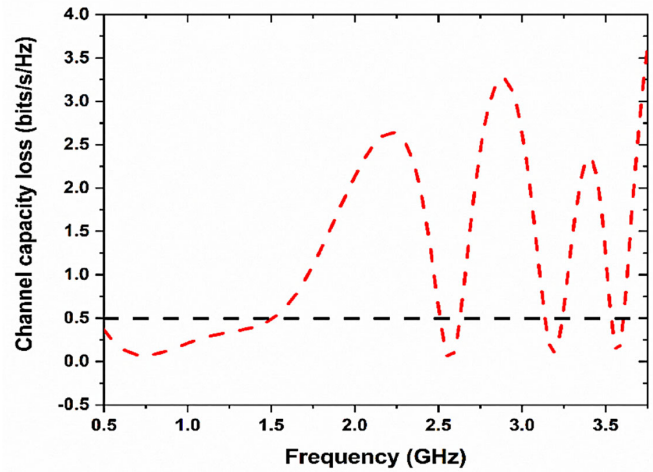

FIGURE 8. Diversity gain of the proposed antenna.

FIGURE 9. Diversity gain of the proposed MIMO antenna.

where S_{11} and S_{22} are the input reflection coefficients of both the ports, and S_{12} is the coupling between the ports. The value of the ECC should be as low as possible to ensure a high coupling between the radiating elements. The ECC variations with frequency are shown in Figure 7. The value should be less than 0.5, and it has been observed from Figure 7 that the ECC value < 0.5 in all the operating frequency bands.

3.2. Diversity Gain (DG)

Diversity gain quantifies the reduction in transmission power required when diversity techniques are implemented on the module, as defined in Equation (6) [15]. Figure 8 demonstrates that the DG for the group of interest remains approximately 10 dB, indicating consistent and effective performance of the diversity scheme.

$$DG = 10\sqrt{1 - |ECC|^2} \qquad (6)$$

3.3. Channel Capacity Loss (CCL)

CCL provides detailed insights into the system's performance based on correlation effects, as described in Equations (7)–(10) [15]. The corresponding values are illustrated in Figure 9, which shows that the CCL remains below 0.5 bits/s/Hz in the frequency bands of interest. This indicates that the proposed antenna achieves high throughput, ensuring its suitability for the intended application.
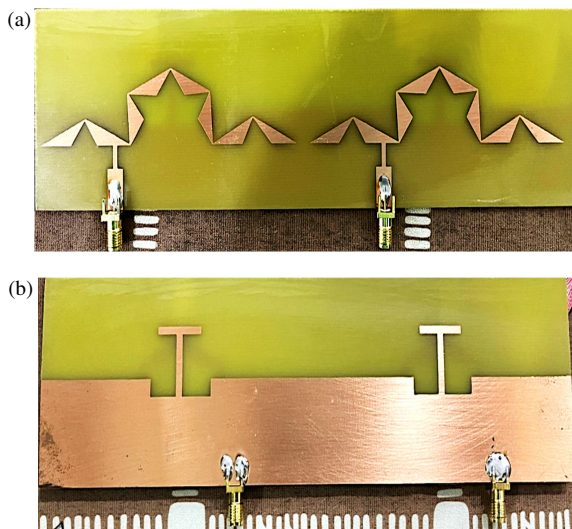
$$C(\text{loss}) = -\log_2 \det(a) \qquad (7)$$

$$a = \begin{bmatrix} \sigma_{11} & \sigma_{12} \\ \sigma_{21} & \sigma_{22} \end{bmatrix} \qquad (8)$$

$$\sigma_{ii} = 1 - \left(|S_{ii}|^2 - |S_{ij}|^2 \right) \qquad (9)$$

$$\sigma_{ij} = -\left(S_{ii}^* S_{ij} + S_{ji} S_{jj}^* \right) \qquad (10)$$
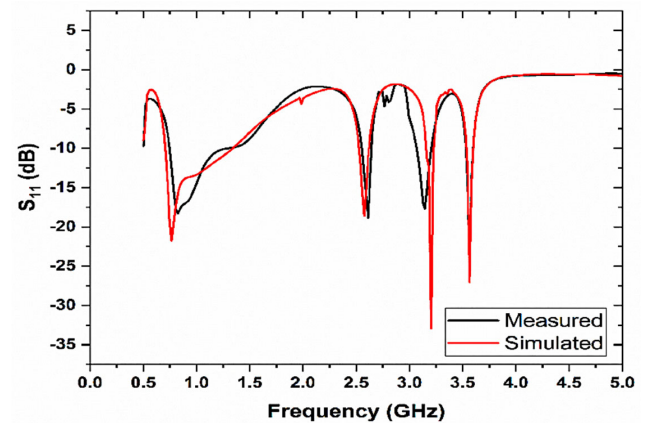
TABLE 3. Comparison of proposed design with recent literature.

References	Operating Frequencies (GHz)	Bandwidth (MHz)	Gain (dBi)	Diversity Gain (dB)	Mutual Coupling (dB)	ECC	Applications
[12]	2.43 3.83 4.4 5.8	2.24–2.5 3.6–3.99 4.4–4.6 5.71–5.90	$>= 2$	9.5–10	$<= -10$	< 0.08	WLAN/WiMAX, Wi-Fi, Bluetooth, C-band
[14]	3	2.21–6	0.53	9.9–10	$<= -15$	< 0.016	Sub-6 GHz 5G and WLAN, IoT
[15]	7.5 10	2.84–11	> -15	-	7.2	< 0.02	Portable and UWB
[16]	2.4	100	2.8–3.52	-	$<= -25$	0.022	2.4 GHz WLAN
[19]	4.8	3.15–5.61(2.46)	2.36		-	-	Low frequency 5G applications
[20]	3.82	2240	4	10	$<= -11$	-	Portable wireless routers/adaptors for 4G and 5G
Proposed Work	0.7 2.6 3.1 3.5	530 110 150 100	7.9 10.2 11.6 12.9	10	$<= -20$ $<= -30$ $<= -40$ $<= -50$	0.001	Low frequency automotive applications

FIGURE 10. Fabrication prototype of the proposed antenna. (a) Top view. (b) Bottom view.

FIGURE 11. Simulated and measured S_{11} (dB) vs frequency of the proposed antenna.

4. FABRICATION AND MEASURED RESULT ANALYSIS

Figure 10 presents the fabricated sample of the proposed MIMO fractal antenna array. The simulated and measured S_{11} (in dB) are depicted in Figure 11, showing good agreement overall, with minor variations observed at 0.7 GHz and 3.1 GHz. Additionally, the radiation patterns of the proposed design, illustrated in Figure 12, demonstrate a high degree of concordance between the measured and simulated results in both co-polarization and cross-polarization planes, confirming the design's robustness and accuracy.

The simulated and measured gains versus frequency plot is shown in Figure 13, which depicts that the measured gain values are less than the simulated values. Because simulations are performed in the ideal boundary conditions and optimized environment. However, during fabrication and measurement, there are certain factors that play significant roles. The factors include fabrication imperfections, material loss, environmental interactions, connector and feed network loss, very sharp edges in the proposed design, and impedance mismatch.
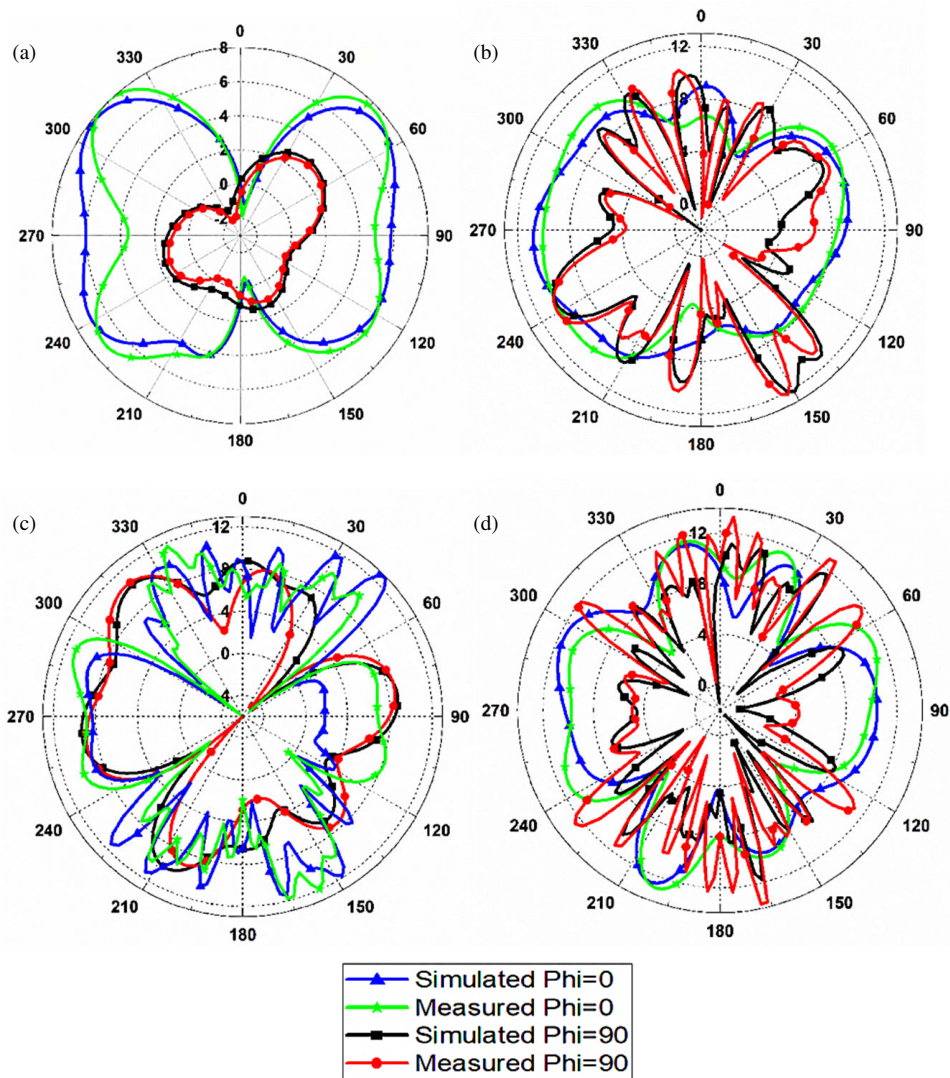
FIGURE 12. Radiation patterns, (a) 0.7 GHz, (b) 2.6 GHz, (c) 3.1 GHz, (d) 3.5 GHz.
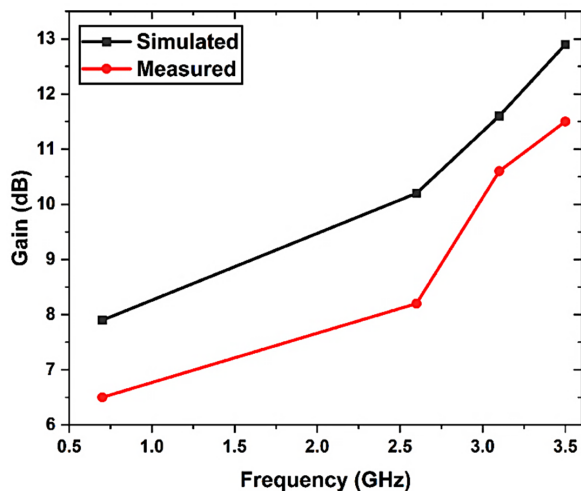

FIGURE 13. Comparison of simulated and measured gains of the proposed antenna at resonating frequencies.

The proposed MIMO antenna design, as highlighted in Table 3, outperforms other referenced works in several key parameters. It achieves a significantly higher gain, reaching up to 12.9 dBi, and demonstrates exceptional mutual coupling performance of ≤ -50 dB, ensuring excellent isolation between antenna elements. The design's envelope correlation coefficient (0.001) is remarkably lower than other designs, as shown in the table, indicating highly uncorrelated MIMO channels for enhanced throughput and reliability. Furthermore, it offers wide bandwidth across multiple operating frequencies, such as 530 MHz at 0.7 GHz, and a diversity gain of 10 dB, matching or surpassing the best values reported in the literature. Unlike other antennas, the proposed design is specifically tailored for low-frequency automotive applications, with practical integration into plastic car body parts, making it ideal for real-world deployment. These advantages, summarized in Table 3, demonstrate the superior versatility and performance of the proposed antenna in applications like 5G, IoT, and automotive communication.

5. CONCLUSION

This paper presents a 1×2 MIMO fractal antenna system for sub-6 GHz 5G automotive applications. The single element fractal antenna is finalized with various iterations, and then the unit cell is transformed into a MIMO configuration to improve the overall channel capacity of the system. The proposed design achieves an excellent impedance bandwidth in the sub-6 GHz frequency bands and maximum gain of around 13 dB in n78 frequency band. The proposed design also achieves the significant coupling between the elements and shows excellent performance in all the MIMO parameters. With these parameters, the proposed design accomplishes acceptable data rate values considering the low earth orbit satellite constellations according to link budget calculations. The achieved data rate will be utilized for various 5G wireless automotive applications.

ACKNOWLEDGEMENT

REFERENCES

[1] Benkhadda, O., M. Saih, S. Ahmad, A. J. A. Al-Gburi, Z. Zakaria, K. Chaji, and A. Reha, "A miniaturized tri-wideband sierpinski hexagonal-shaped fractal antenna for wireless communication applications," *Fractal and Fractional*, Vol. 7, No. 2, 115, 2023.

[2] 3GPP TS 38.101-4, "Technical specifications group radio access network; NR; User equipment (UE) radio transmission and reception; part 4: performance requirements," v.17.3.0, 2022.

[3] Del Portillo, I., B. G. Cameron, and E. F. Crawley, "A technical comparison of three low earth orbit satellite constellation systems to provide global broadband," *Acta Astronautica*, Vol. 159, 123–135, 2019.

[4] Elabd, R. H. and A. J. A. Al-Gburi, "Design and optimization of a circular ring-shaped UWB fractal antenna for wireless multiband applications using particle swarm optimization," *Progress In Electromagnetics Research B*, Vol. 106, 101–112, 2024.

[5] Abdullah Al-Gburi, A. J., "5G MIMO antenna: Compact design at 28/38 GHz with metamaterial and SAR analysis for mobile phones," *Przeglad Elektrotechniczny*, Vol. 2024, No. 4, 171–174, 2024.

[6] Sim, C.-Y.-D., H.-Y. Liu, and C.-J. Huang, "Wideband MIMO antenna array design for future mobile devices operating in the 5G NR frequency bands n77/n78/n79 and LTE band 46," *IEEE Antennas and Wireless Propagation Letters*, Vol. 19, No. 1, 74–78, Jan. 2020.

[7] Kumar, A., H.-P. Petry, U. Tayyab, and M. A. Hein, "Link budget considerations for automotive 5G LEO satellite-based communications," in *2022 IEEE USNC-URSI Radio Science Meeting (Joint with AP-S Symposium)*, 106–107, Denver, CO, USA, 2022.

[8] Arif, A., M. Zubair, M. Ali, M. U. Khan, and M. Q. Mehmood, "A compact, low-profile fractal antenna for wearable on-body WBAN applications," *IEEE Antennas and Wireless Propagation Letters*, Vol. 18, No. 5, 981–985, May 2019.

[9] Kumar, P., A. K. Singh, R. Kumar, S. K. Mahto, P. Pal, R. Sinha, A. Choubey, and A. J. A. Al-Gburi, "Design and analysis of low profile stepped feedline with dual circular patch MIMO antenna and stub loaded partial ground plane for wireless applications," *Progress In Electromagnetics Research C*, Vol. 140, 135–144, 2024.

[10] Pedram, K., J. Nourinia, C. Ghobadi, N. Pouyanfar, and M. Karamirad, "Compact and miniaturized metamaterial-based microstrip fractal antenna with reconfigurable qualification," *AEU — International Journal of Electronics and Communications*, Vol. 114, 152959, 2020.

[11] Thakur, E., A. Gupta, M. K. Abdulhameed, A. D. Khaleel, and A. J. A. Al-Gburi, "Microstrip antenna with two elements and defected ground structure for 5G mobile applications at 28/38 GHz," *Progress In Electromagnetics Research C*, Vol. 146, 177–185, 2024.

[12] Chouhan, S., D. K. Panda, V. S. Kushwah, and S. Singhal, "Spider-shaped fractal MIMO antenna for WLAN/WiMAX/Wi-Fi/Bluetooth/C-band applications," *AEU — International Journal of Electronics and Communications*, Vol. 110, 152871, 2019.

[13] Khalid, M., S. I. Naqvi, N. Hussain, M. Rahman, Fawad, S. S. Mirjavadi, M. J. Khan, and Y. Amin, "4-port MIMO antenna with defected ground structure for 5G millimeter wave applications," *Electronics*, Vol. 9, No. 1, 71, 2020.

[14] Desai, A., M. Palandoken, J. Kulkarni, G. Byun, and T. K. Nguyen, "Wideband flexible/transparent connected-ground MIMO antennas for sub-6 GHz 5G and WLAN applications," *IEEE Access*, Vol. 9, 147 003–147 015, 2021.

[15] Addepalli, T., A. Desai, I. Elfergani, N. Anveshkumar, J. Kulkarni, C. Zebiri, J. Rodriguez, and R. Abd-Alhameed, "8-port semi-circular arc MIMO antenna with an inverted L-strip loaded connected ground for UWB applications," *Electronics*, Vol. 10, No. 12, 1476, 2021.

[16] Li, H., J. Xiong, and S. He, "A compact planar MIMO antenna system of four elements with similar radiation characteristics and isolation structure," *IEEE Antennas and Wireless Propagation Letters*, Vol. 8, 1107–1110, 2009.

[17] Rian, I. and M. Sassone, "Fractal-based generative design of structural trusses using iterated function system," *International Journal of Space Structures*, Vol. 29, No. 4, 181–203, 2014.

[18] ETSI, "TS 38.101-1: NR; User Equipment (UE) radio transmission and reception; Part 1: Range 1 Standalone (18.3.0 ed.). 3GPP," 2023.

[19] Azim, R., T. Alam, L. C. Paul, R. Aktar, A. K. M. M. H. Meaze, and M. T. Islam, "Low profile multi-slotted patch antenna for lower 5G application," in *2020 IEEE Region 10 Symposium (TENSYMP)*, 366–369, Dhaka, Bangladesh, 2020.

[20] Sarkar, D. and K. V. Srivastava, "A compact four-element MIMO/diversity antenna with enhanced bandwidth," *IEEE Antennas and Wireless Propagation Letters*, Vol. 16, 2469–2472, 2017.

[21] Dhasarathan, V., T. K. Nguyen, M. Sharma, S. K. Patel, S. K. Mittal, and M. T. Pandian, "Design, analysis and characterization of four port multiple-input-multiple-output UWB-X band antenna with band rejection ability for wireless network applications," *Wireless Networks*, Vol. 26, 4287–4302, 2020.

[22] Kumar, G. and R. Kumar, "A survey on planar ultra-wideband antennas with band notch characteristics: Principle, design, and applications," *AEU — International Journal of Electronics and Communications*, Vol. 109, 76–98, 2019.